Earthquakes and Structures, Vol. 3, No. 5 (2012) 767-781
DOI: http://dx.doi.org/10.12989/eas.2012.3.5.767

Seismic damage of long span steel tower suspension bridge considering strong aftershocks

X. Xie*[1], G. Lin[1], Y.F. Duan[1], J.L. Zhao[1] and R.Z. Wang[2]

[1]*Department of Civil Engineering, Zhejiang University, Hangzhou, 310058, China*
[2]*Center for Research on Earthquake Engineering, Taipei, 10668, Taiwan, China*

(Received January 31, 2011, Revised December 28, 2011, Accepted April 23, 2012)

Abstract. The residual capacity against collapse of a main shock-damaged bridge can be coupled with the aftershock ground motion hazard to make an objective decision on its probability of collapse in aftershocks. In this paper, a steel tower suspension bridge with a main span of 2000 m is adopted for a case-study. Seismic responses of the bridge in longitudinal and transversal directions are analyzed using dynamic elasto-plastic finite displacement theory. The analysis is conducted in two stages: main shock and aftershocks. The ability of the main shock-damaged bridge to resist aftershocks is discussed. Results show that the damage caused by accumulated plastic strain can be ignored in the long-span suspension bridge. And under longitudinal and transversal seismic excitations, the damage is prone to occur at higher positions of the tower and the shaft-beam junctions. When aftershocks are not large enough to cause plastic strain in the structure, the aftershock excitation can be ignored in the seismic damage analysis of the bridge. It is also found that the assessment of seismic damage can be determined by superposition of damage under independent action of seismic excitations.

Keywords: long-span suspension bridge; steel tower; main shock; aftershock; seismic damage

1. Introduction

Series of strong aftershocks after the main shock make the structure suffer from strong earthquakes successively in a short time. For instance, there are two strong aftershocks with peak accelerations larger than 0.5 g (g: acceleration of gravity) in the first 60 seconds as recorded at Wolong station during Wenchuan Earthquake in China on May 12, 2008 (Zhao and Taucer 2010). An aftershock of M 6.1 struck 15 hours after the main shock (M 7.8) during Tangshan Earthquake in China in 1976 (George). An aftershock with the magnitude of M 6.5 occurred one hour after the main shock of Niigata Chuetsu Earthquake (M 6.8) in Japan in 2004 (Japan Meteorological Agency 2004). The magnitude of the main shock of Taiwan Chi-Chi Earthquake (921 Earthquake) is M 7.3, and the aftershock of M 6.8 happened within one hour after the main shock which made more infrastructure damage than the main shock did (Kim *et al*. 1999). Although the intensity of the aftershock is generally smaller than that of the main shock and the structure may withstand the main shock without severe damage, the following aftershocks may cause further damage in structures, because the epicenters of the main- and after-shocks are close and the capacity of the

*Corresponding author, Professor, E-mail: xiexu@zju.edu.cn

structure is reduced after the main shock.

Up to now, there are few studies on the seismic performance of bridges considering the action of aftershocks. Amadio *et al*. (2003) and Fragiacomo *et al*. (2004) analyzed the effects of repeated earthquake ground motions on the response of single degree of freedom (SDOF) systems with nonlinear behavior. Franchin and Pinto (2009) proposed a criterion for deciding whether a bridge can still be open for either emergency or ordinary traffic after a strong main shock based on aftershock probabilistic seismic hazard analysis. Kimura *et al.* (2007) studied the structural cumulative seismic damage of a SDOF reinforced concrete bridge pier taking into account both main- and after-shocks. Li and Ellingwood (2007) conducted a probabilistic damage assessment for steel frame buildings under main- and after-shock earthquake sequence using the enhanced uncoupled modal response history analysis method. Murata *et al.* (2004) investigated the destructive power on wooden structures using response spectra considering the number of seismic response cycles. Luco *et al.* (2004) proposed a "calibrated" static approach for computing the residual capacities of a main shock-damaged building through nonlinear static-pushover analysis, in terms of the aftershock ground motion that the building can withstand without collapse. Lee and Foutch (2004) presented a systematic evaluation approach to estimate the performance of damaged buildings subjected to sets of ground motions representing different hazard levels.

The post-earthquake serviceability and reparability of bridges are critical factors in traffic lifeline, as well as the performance requirements of seismic design. Long-span suspension bridges are long span structures with complex seismic response characteristics. The seismic damage mode, the post-earthquake serviceability and reparability of such structures have not been made clear. This paper aims to investigate the structural seismic damage of long-span suspension bridges under both main- and after-shocks based on the seismic responses of a super-long suspension bridge with a main span of 2000 m using dynamic elasto-plastic finite displacement theory. Distinguished from others, this paper will study the whole long-span complex bridge structure rather than a SDOF model or simple structural components, using the real-world earthquake records of main- and after-shocks rather than artificial main- and after-shock excitations.

2. The studied bridge and ground motions

2.1 The bridge model

In this study, a suspension bridge with a main span of 2000 m is employed. Fig. 1 shows a side-view of the bridge, a front-view and cross-section of the tower. The span arrangement is 1000 m + 2000 m + 1000 m. Steel towers and a flat steel box girder with two separate boxes are adopted. The height of the tower from the foundation top is 280 m, and the distance between the two tower shafts is 40 m at the base, and 24 m at the top. The section of each tower shaft consists of a single box with three cells, as shown in Fig. 1(b). The section height of the tower shaft reduces gradually from 13 m at the base to 8 m at the top; the steel plate thickness varies from 58 mm at the base to 38 mm at the top; and the section area changes from 2.131 m^2 at the base to 3.725 m^2 at the top. The two tower shafts are connected by cross beams. The section of the cross beams of the main tower is also given in Fig. 1(b); the steel plate thickness varies from 30 mm to 40 mm. The main cables consist of parallel wires, the rise-span ratio of which is about 1/9.2 and the distance between the two main cables is 24 m. Hangers are installed with a uniform 30 m spacing. Table 1 shows the

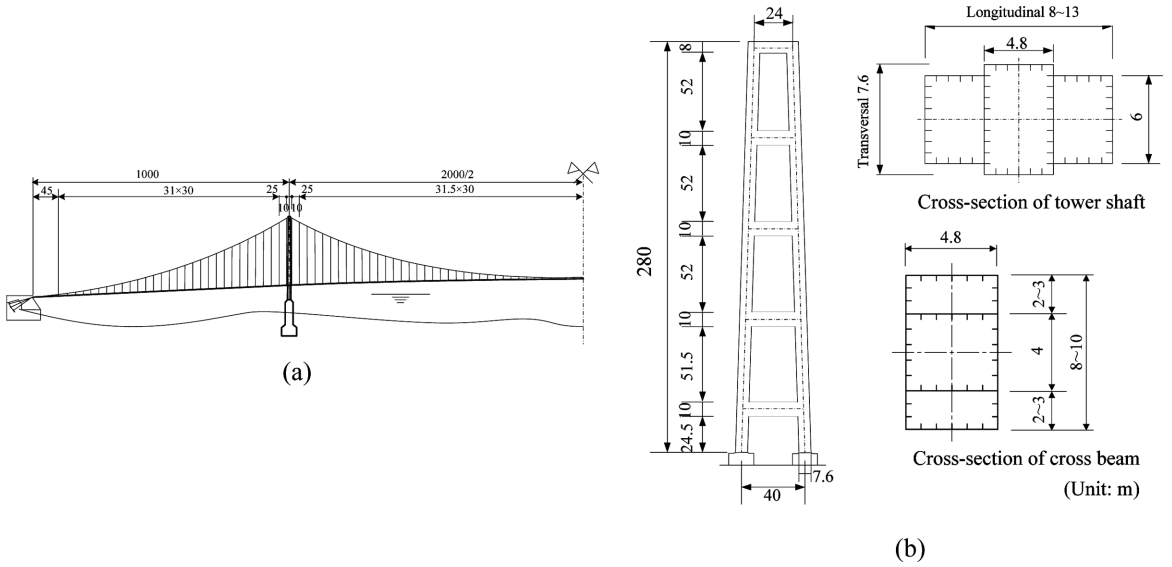

Fig. 1 The suspension bridge model: (a) side view of the bridge (half bridge) and (b) front view of the tower and cross-section of tower shafts and cross beams

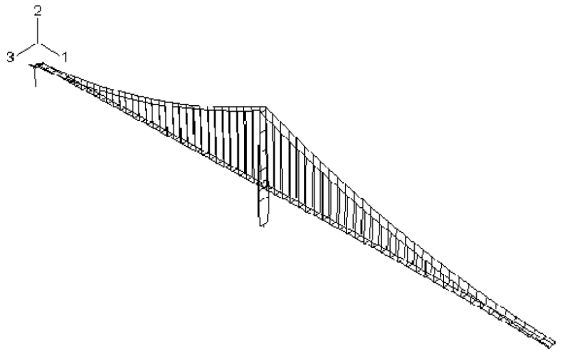

Fig. 2 3-D analytical model of the bridge (half bridge)

Table 1 Cross-section properties of structual members

Parameter	Main cable/single	Suspender/single	Stiffening girder/single	Tower/tower shaft
A (m^2)	0.367	0.00627	0.388	2.119~3.706
I_x (m^4)	--	--	0.610	14.376~26.582
I_y (m^4)	--	--	3.350	17.567~66.369
K (m^4)	--	--	1.980	16.515~42.331

main parameters of the structure, in which A, I_x, I_y and K are the sectional area (m^2), inertia moment about the horizontal axis in transveral direction (m^4), inertia moment about the other principal axis (m^4) and torsional constant (m^4). The cross-sectional parameters are determined by structrual preliminary design. The suspension bridge meets the stress and deformation requirements of Japan code of highway bridges (Japan Road Association 2002) under design live loads mainly. The initial

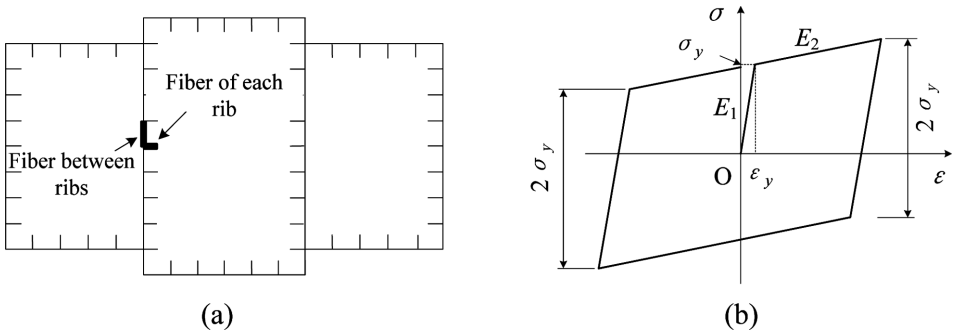

Fig. 3 Fiber elements of tower shafts and stress-strain relationship of steel: (a) fiber elements of the tower shafts and (b) stress-strain relationship of steel

axial force of the main cable at the stage of completion is 2.90×10^5 kN to 3.22×10^5 kN, and the initial axial force of the tower is 2.56×10^5 kN to 3.48×10^5 kN.

A 3-D analytical model, using the general finite element (FE) progeam Abaqus6.5/Standard (Abaqus 2006) is carried out for seismic response analysis as shown in Fig. 2. The stiffening girders are modelled with 3-D elastic beam element (B31) and main cables and hangers are modelled with 3-D truss element (T3D2). The main shafts and cross beams are modelled with 3-D elasto-plastic beam element in order to consider the seismic damage, and the interactions between soil and the structure are simulated by foundation springs. The cross beam element connects the shaft element by a horizontal rigid beam which is used to consider the effect of sectional height of the tower shaft.

In order to consider the plasticity development in the tower and the effect of axial force on the structural seismic responses, the towers (including cross beams) are modelled with fiber element. Fig. 3(a) shows the fiber division of the tower shaft cross-section. Every stiffening rib and every strip of the steel plates between neighbouring longitudinal stiffening ribs or between the stiffening ribs and the conner plates represent one piece of fiber, respectively. There are 44 pieces of fiber on the cross-section at the top of each tower shaft, and 52 pieces at the base. The uniaxial stress-strain curve of the steel is bilinear elasto-plasitc model as shown in Fig. 3(b), of which the post-yield modulus (E_2) is 1% of the initial elastic modulus (E_1) accounting for steel hardening. The hardening rule is based on the kinematic hardening model. σ_y and ε_y in the figure are yield stress and yield strain, respectively. The elastic modulus and yield stress of the steel are 2.0×10^5 MPa and 450 MPa, respectively. The elastic modulus of cables is 1.99×10^5 MPa.

2.2 Seismic characteristics of main- and after-shocks

Currently, the correlation between main- and after-shocks has not been clearly defined in bridge seismic design specifications. According to relevant literature, the frequency characteristics of response spectrum curves of aftershocks are close to those of main shocks (Franchin and Pinto 2009). The authors collected five records of main shocks and aftershocks recorded at different locations during three earthquakes. The horizontal (EW or NS) and vertical (UD) peak accelerations of these five records are shown in Table 2. Record 1 is obtained at Sun Moon Lake observation point during Chi-Chi Earthquake in Taiwan in 1999, for which the magnitude of the main shock is M 7.3, and that of the aftershock is M 6.7. Record 2 is recorded at Urakawa-cho observation point

Table 2 Peak acceleration of main shock and aftershock

Record No.	Earthquake	Observation location	Main shock (m/s^2)		Aftershock (m/s^2)	
			EW (NS)	UD	EW (NS)	UD
1	Chi-Chi	Sun Moon Lake	9.89	3.12	3.10	1.19
2	Tokachi-oki	Urakawa town	3.49	0.98	4.93	0.77
3	Chuetus	Kawaguchi town	16.76	8.70	20.36	5.49
4	Chuetus	Tokamachi	17.13	5.68	8.14	2.25
5	Chuetus	Ojiya	11.39	8.18	7.84	3.51

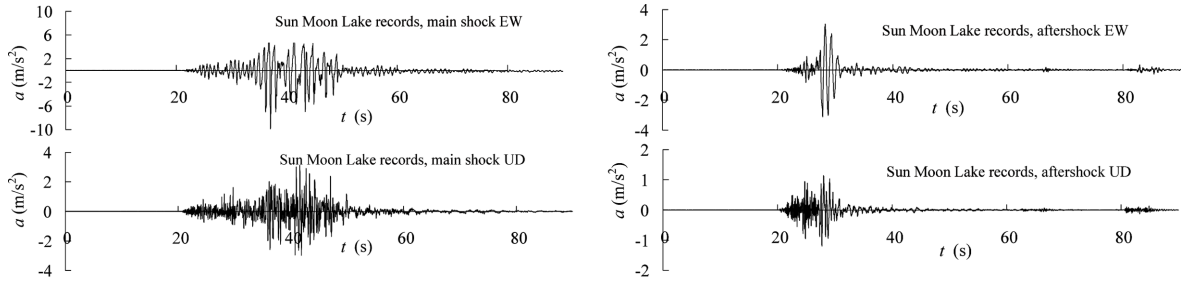

(a) (b)

Fig. 4 Sun Moon Lake record of Chi-Chi Earthquake in Taiwan (1999): (a) main shock and (b) aftershock

during Tokachi-oki Earthquake in Japan in September of 2003, for which the magnitude of the main shock and aftershock is M 8.0 and M 7.1, respectively. Record 3 to 5 are obtained from different observation points duing Chuetus Earthquake on 23 October, 2004, in Niigata, Japan, for which the magnitude is M 6.8 for the main shock and M 7.1 for the aftershock. It is indicated that the peak acceleration of aftershocks may be equal to, or even larger than that of main shocks. For instance, the Kawaguchi Town record in Niigata Chuetsu Earthquake (Record 3) shows that the magnitudes of both main shock and aftershock exceeded 1.0 g, and the peak horizontal acceleration of the aftershock reached 20.36 m/s^2, which is larger than that of the main shock of 16.76 m/s^2.

By analyzing the spectra of these 5 records, it is found that the predominant period of Sun Moon Lake record of Chi-Chi Earthquake is relatively long, while that of Chuetus Earthquake is short and the duration of its strong aftershock is short. For long span suspension bridges, the long duration of strong seismic action and long-period components of ground motion are significant factors to induce large seismic reposonses. Based on this principle, this paper adopted the Sun Moon Lake record (Fig. 4) of Chi-Chi Earthquake as the seismic input to study the seismic damage of the long span suspension bridge. Meanwhile, it is seen from the comparison of the peak accelerations between main shocks and aftershocks of the other four recods of seismic waves that the peak acceletation of aftershocks may be greater than that of main shocks. Considering the aftershock magnitude of the Sun Moon Lake record is relatively small, it is amplified by 1 to 3 times in the computation so that the peak acceleration of the aftershock reaches or even exceeds that of the main shock in order to study the aftershock effect on seismic damage of suspension bridges.

Fig. 5 shows the response spectra of the Sun Moon Lake record (damping ratio 5%). It is clear that the frequency characteristics of the main shock and aftershocks are similar to some extent. The

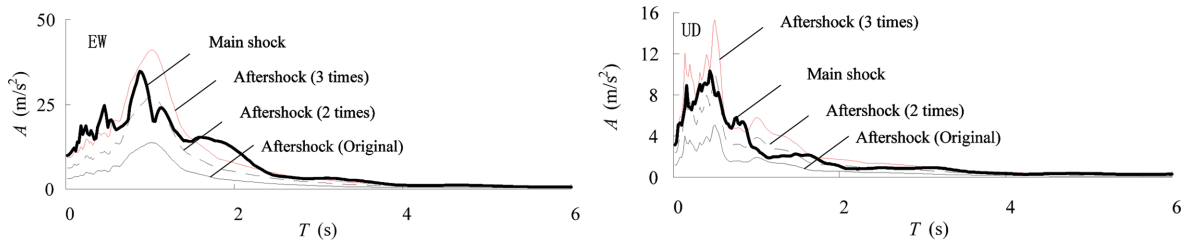

(a) (b)

Fig. 5 Response spectra of the seismic input: (a) response spectra in horizontal direction and (b) response spectra in vertical direction

response spectrum acceleration exceeds that of the main shock when the aftershock magnitude is enlarged to 3 times.

3. Evaluation methods of structural seismic damage

The ratio of maximum strain response to ultimate strain is usually taken as the basis in seismic safety verification of bridge structures. However, this method ignores the effect of cumulative damage during the earthquake despite the merits of intuition and simplicity.

In order to consider the effect of cumulative damage, some scholars proposed seismic damage indices to evaluate the structural damage level, in which the maximum earthquake deformation damage and cumulative energy dissipation are considered together, based on the view that structures dissipate seismic energy by absorbing it. Park and Alfredo (1985) defined the seismic damage index of reinforced concrete structures using linear combination of the maximum displacement and the cumulative energy dissipation according to the experimental results of structural components under cyclic loading. In this paper in order to consider the cumulative effect, the seismic damage indices are established based on the low-cycle fatigue theory of McCabe and Hall (1989). Because the ultimate compressive strain of steel structures is related to design details, for simpilty and without losing generality this paper uses plastic rate to describe the structural damage instead of ultimate compressive strain without considering the design details. Two simple indices are used to indicate the seismic damage of the steel towers:

$$\left.\begin{aligned} D_1 &= \frac{\varepsilon_M}{\varepsilon_y} \\ D_2 &= C\sum_{i=1}^{n}(\Delta\varepsilon_{pi})^m \end{aligned}\right\} \tag{1}$$

where ε_y, ε_M and n are the yield strain, the maximum strain and the number of loading cycles, respectively. $\Delta\varepsilon_{pi}$ is the plastic strain increment of cycle i in response history as shown in Fig. 6. According to related experimental results, coefficient C is assumed to be 1.57, and the exponent m is 1.7 (Usami 2007).

Fig. 7 shows the general relation between the structural damage level and damage index D_1.

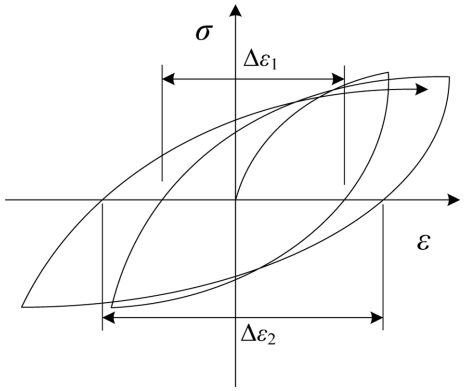

Fig. 6 Definition of the cumulative plastic strain

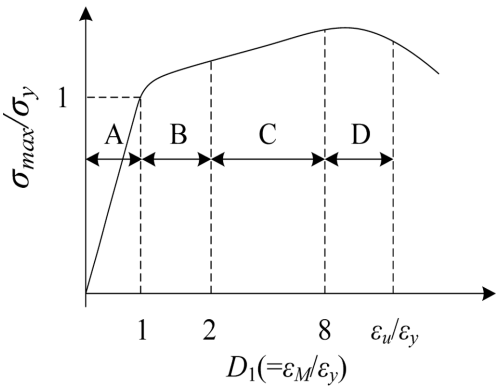

Fig. 7 Relation between damage level and damage index D_1

Region A-D represent no damage, slight damage, reparable damage and severe damage, respectively. And the cumulative index D_2 indicates material state: when the value of D_2 equals to 1.0, it represents the material has reached its limit state. The index D combining the above two damage indices should be

$$D = \frac{D_1}{8} + D_2 \tag{2}$$

When D equals to 1.0, it means the structure reaches the failure limit state (Park and Alfredo 1985).

4. Seismic responses of the long-span suspension bridge

The vibration mode shapes of the long-span suspension bridge are very complex, with horizontal earthquake action coupling with vertical one, and P-Δ effect will cause additional bending moment in tower which may lead to structural instability. Therefore, direct integration method is applied considering both material and geometric nonlinearities. In order to reduce the computing time, only 20-70 s segments of the main- and after-shock waves are used as seismic input.

4.1 Structural natural vibration characteristics

The natural vibration characteristics of the bridge are calculated using subspace iteration method. The first 10 natural frequencies and corresponding mode shapes are shown in Table 3. Due to the flexible feature of long-span structures, the natural frequencies of lower modes of the long-span suspension bridges are very small. The period of the 1st natural mode (1st lateral bending mode) is 27.7 s. The natural frequency of the first symmetric vertical bending mode is 0.065032 Hz, and its corresponding period is 15.38 s. In addition, tower vibration modes did not appear in the first 10 vibration modes.

Table 4 lists the modes with obvious tower bending vibration of the first 200 modes and their

Table 3 The first 10 vibration modes of the bridge

Modal order	Modal frequency (Hz)	Characteristics of mode shape
1st	0.036073	1st symmetric lateral bending of main span
2nd	0.064484	1st antisymmetric lateral bending of main span
3rd	0.065032	1st symmetric vertical bending of full-bridge
4th	0.069742	1st symmetric lateral bending of left side span
5th	0.071276	1st antisymmetric vertical bending of full bridge
6th	0.086411	longitudinal drift of left side span
7th	0.092759	1st symmetric lateral bending of right side span
8th	0.095645	longitudinal drift of right side span
9th	0.101655	2nd symmetric lateral bending of main span
10th	0.113979	2nd symmetric vertical bending of full-bridge

Table 4 Major modes and participation factor of tower vibration

Modal order	Frequency (Hz)	Participation factor
46th	0.33978	2.2356
49th	0.34351	0.2592
76th	0.56355	0.4481
91st	0.65183	0.1937
98th	0.68729	1.6247
141st	1.00110	0.0087
182nd	1.32210	0.8710
193rd	1.40840	0.0605

modal participation factors in longitude direction. From the frequencies in Table 4 and the response spectra in Fig. 5, it is seen that the periods of most tower modes correspond to large ordinate values in response spectra. As a result, the seismic effect on towers will be significant.

4.2 Seismic responses under longitudinal seismic excitation

In order to investigate aftershock effect in longitudinal direction on seismic damage of the long-span suspension bridge, the horizontal ground motions are input in longitudinal direction of the bridge as well as the vertical ground motions input in vertical direction.

Fig. 8 shows the distribution of plastic regions (dark parts in the figures) at the end of the main shock and aftershocks. The results show that the plastic regions develop in the tower at the height of the second cross beam and at the base of the tower shafts. The development of plastic regions under aftershocks depends on the intensity of the aftershocks. When the input aftershock is the original record, no new plastic region appears during the aftershock; however, when the aftershock is 2 or 3 times of the original record, new plastic regions appear expanding the area of the main shock plastic regions, but the locations of the plastic regions keep unchanged. The reason that the plastic regions occur at high position of the tower lies in that the horizontal movement at the top of the tower is constrained by the main cables, resulting in the tower boundary condition of

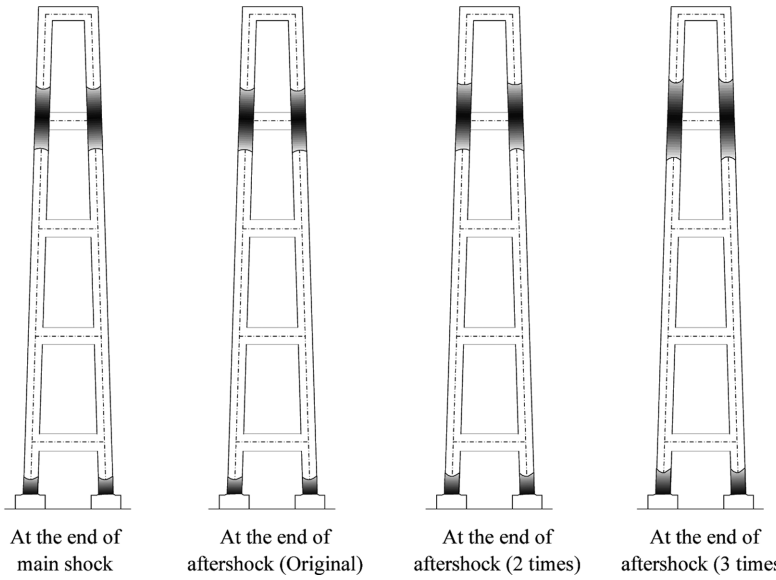

Fig. 8 Distribution of plastic regions after main shock and aftershocks with different amplification factors

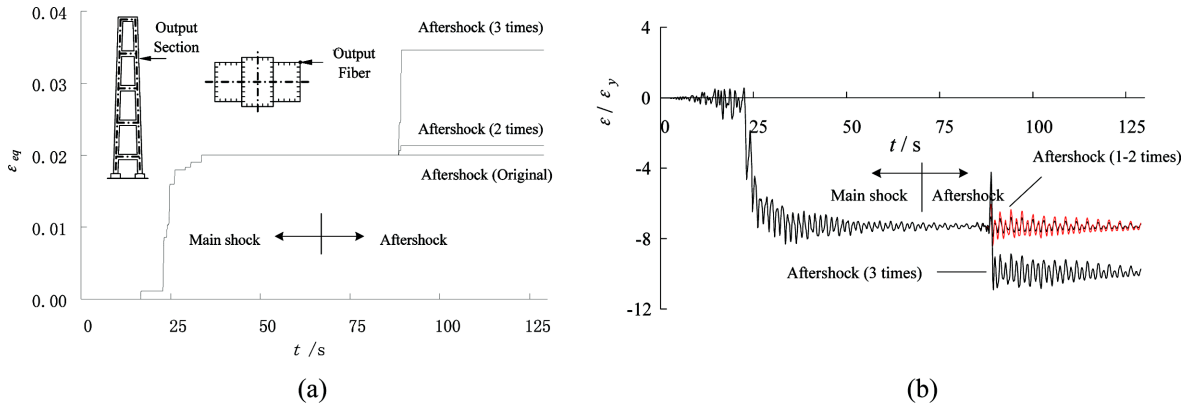

Fig. 9 Strain responses of the fiber with maximum plastic strain under longitudinal earthquake: (a) equivalent plastic strain and (b) plastic rate

approximately being fixed at the bottom and hinged at the top.

Fig. 9 shows the history of equivalent plastic strain ε_{eq} and relative strain ($\varepsilon/\varepsilon_y$) at the fiber with maximum plastic strain (see dark parts in Fig. 8). Within the first 15 seconds of the main shock, the structure responds in elastic range due to relatively small seismic excitation and no plastic strain occurs. From 18 s to 35 s, the seismic intensity increses to its maximum value, and plastic strain occurs. After 35 s, with the weakening of the earthquake, no new plastic strain develops. Throughout the process of the main shock, the maximum equivalent plastic strain is 2.00%, and the absolute relative strain is 8.31 with large residual strain occurring. According to the general definition of structural damage in Fig. 7, it can be inferred that serious damage has occurred to the tower after the main shock.

The plastic strain caused by aftershocks depends on the intensity of the aftershocks. As shown in Fig. 9, no new plastic strain develops under the aftershock of original record; the plastic strain increases slightly under the aftershock of 2 times of the original record, while under the aftershock of 3 times, the plastic strain increases significantly and new residual deformation occurs with the absolute relative strain of 10.9 and obviously increased damage index D_1. This suggests that only when the intensity of an aftershock reaches a certain level may the aftershock cause new earthquake damage; otherwise, the effect of aftershocks can be neglected in the seismic design.

Table 5 shows the cumulative damage index D_2 calculated by Eq. (1). It can be seen that the long-span suspension bridge undergoes very small number of displacement cycles due to its long natural period. The seismic damage caused by accumulated plastic strain is far less than 1.0 even under the aftershock of 3 times; thus it will not affect the evaluation of seismic performance.

Fig. 10 shows the longitudinal seismic displacement responses at the tower top (Section A) and at the height of the second cross beam (Section B). The results show that, since serious yield damage appears in the tower shaft, large residual displacement occurs at Section B: 2.0 m due to the main shock, and additionally 0.4 m due to the aftershock of 3 times of the original record. However, the longitudinal displacement of the tower top (Section A) is less than that of Section B as a result of the constraint by the main cables at the top, and the residual displacment is also smaller than that of Section B.

In order to study the effect of the main shock induced damage on the damage caused by aftershocks, the aftershock of 3 times of the original record is used again as the seismic input. Two

Table 5 Cumulative damage index D_2 under longitudinal earthquake

Seismic damage	Mainshock	Main shock + aftershock		
		Aftershock (Original)	Aftershock (2 times)	Aftershock (3 times)
D_2	0.000727	0.000727	0.000739	0.001531

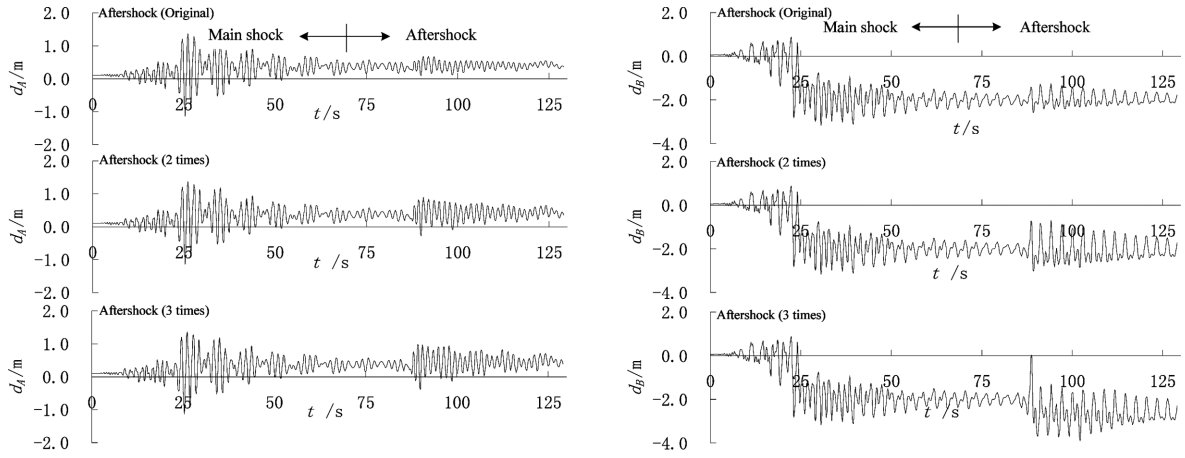

Fig. 10 Displacement responses of the tower under longitudinal earthquake: (a) tower top (Section A) and (b) at the height of the 2nd cross beam (Section B)

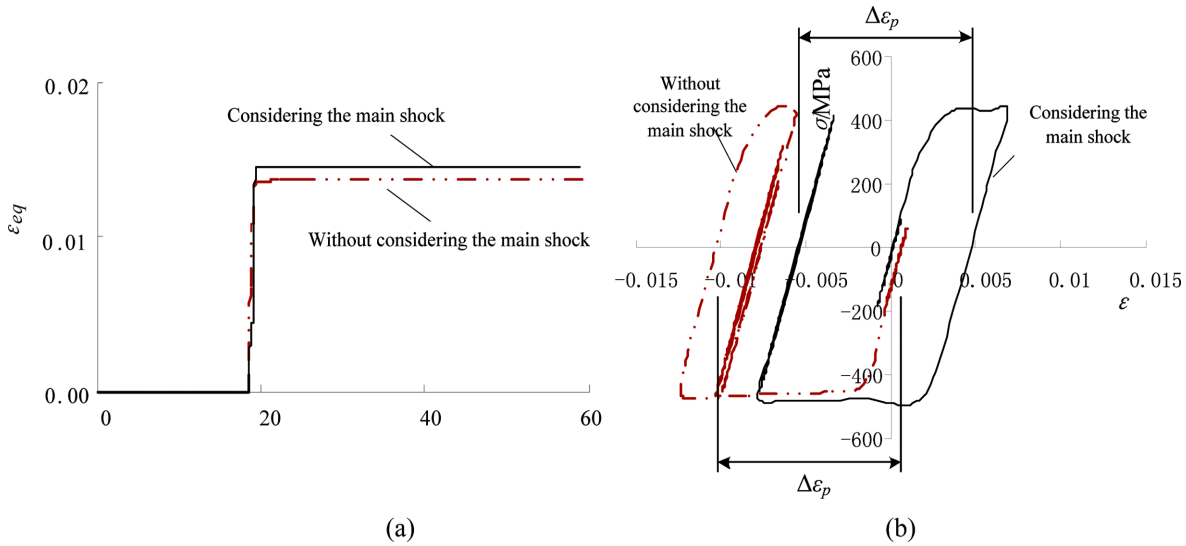

Fig. 11 The effect of longitudinal main shock damage on the strain responses of aftershock: (a) equivalent plastic strain and (b) stress-strain hysteretic curves

cases are analyzed: Case I using the seismic input of the main shock followed by that of the aftershock and Case II using the aftershock seismic input only. Because the result of Case I contains the residual deformation and strain due to the main shock, in order to compare the pure effect of the aftershock in the two cases, the residual effect of the main shock in Case I is removed by translation. Fig. 11 shows the equivalent plastic strain and stress-strain hysteretic curves at the fiber of maximum plastic strain for the two cases. It is seen that both the equivalent plastic strain and the maximum plastic strain increment $\Delta\varepsilon_p$ due to the aftershock are not obviously affected by the main shock, and the results of the two cases are almost the same. This observation indicates that for the studied case the evaluation of damage due to the combined action of main- and after-shocks can be conducted by superposing damage on the original structure under main shocks only and under aftershocks only.

4.3 Seismic responses under transversal seismic excitation

In order to study the effect of aftershocks in transversal direction on seismic damage of long-span suspension bridges, the horizontal ground motions are input in transversal direction of the bridge and the vertical ground motions are input in vertical direction to calculate the structural seismic responses. Fig. 12 shows the plastic regions of the tower, showing that damage at junctions between cross beams and the tower shafts is serious. Compared to the longitudinal seismic damage, the aftershock effect on seismic damage in transversal direction is more significant and the damaged regions expand with the increase of aftershock intensities. This is because that the natural period of the bridge in transversal direction is short and closer to the predominant frequency contents of the ground motion. It is easily seen from the response spectra in Fig. 5 that when the aftershock intensity increases, the seismic action obviously gets stronger.

Fig. 13 shows the history of the equivalent plastic strain at the position of maximum plastic strain.

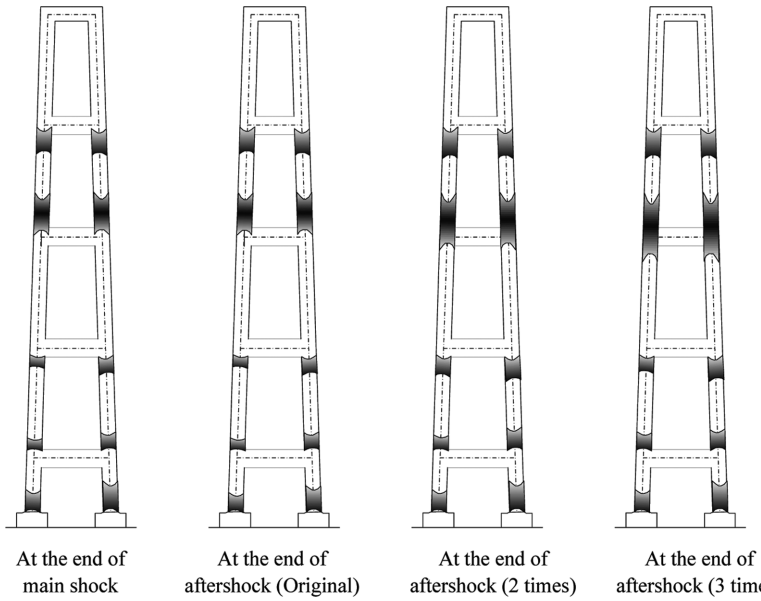

Fig. 12 Distribution of plastic regions after main shock and aftershocks with different amplification factors

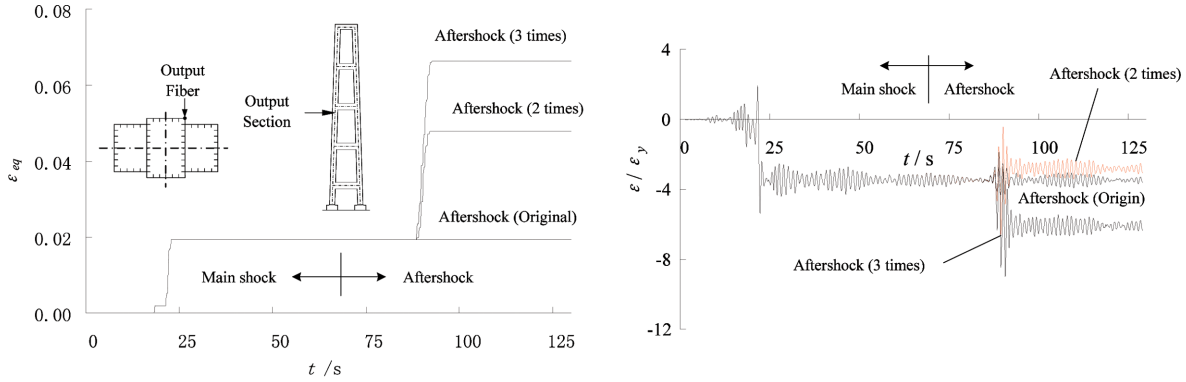

Fig. 13 Strain responses of the fiber with maximum plastic strain under transversal earthquake: (a) equivalent plastic strain and (b) plastic rate

It shows that no new plastic strain develops under the action of the original aftershock, while the equivalent plastic strain increases significantly under aftershocks of 2 times or 3 times. For the aftershock of 2 times, the absolute residual strain is smaller than that of the main shock. The absolute residual plastic strain rate at the end of the main shock is about 3.5, and the additional absolute residual plastic strain rate due to aftershock of 1 to 3 times is 0, 0.6 and 2.7, respectively.

Fig. 14 shows the displacement responses at the tower top (Section A) and at the tower height of the third cross beam (Section C) in transversal direction. The results show that the residual deformation does not occur at the tower top under the main shock, neither under aftershocks of original record and 2 times of the record, but the residual deformation occurs under the aftershock

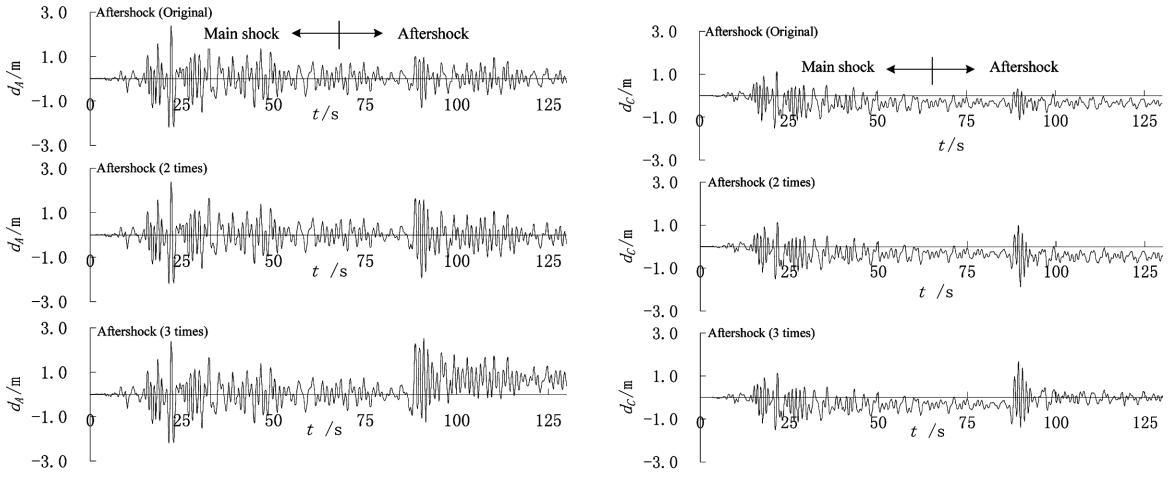

Fig. 14 Displacement response of the tower under transversal earthquake: (a) tower top (Section A) and (b) at the level of the third cross beam (Section C)

Table 6 Cumulative damage index D_2 under transversal earthquake

Seismic damage	Main shock	Main shock + aftershock		
		Aftershock (Original)	Aftershock (2 time)	Aftershock (3 time)
D_2	0.00101	0.00101	0.00227	0.00339

of 3 times. At Section C, the residual deformation of 0.3 m occurs under the main shock, and there is no additional residual deformation occurring due to aftershocks of original record and 2 times of the record. However, as the aftershock intensity reaches 3 times, the additional residual deformation at Section C occurs in the opposite direction to the residual displacement under the main shock.

Table 6 shows the cumulative damage index D_2 under the transversal seismic excitation. It is found that the damage corresponding to the accumulated plastic strain in the transversal direction is also quite small which can be ignored compared with the limit value of 1.0.

In order to study the effect of the main shock induced damage on the seismic response under aftershocks, the aftershock of 3 times of the original record is used again as the seismic input for the investigation. Depending on whether the main shock is considered or not, there are two computation cases: Case I considering the effect of main shock and Case II without considering the main shock. Fig. 15 shows the equivalent plastic strain and the stress-strain hysteretic responses (excluding the main shock induced part). The results show that both the equivalent plastic strain and the maximum plastic strain increment $\Delta\varepsilon_p$ are not obviously affected by the main shock. It shows that the effect of main shock induced damage on seismic responses under aftershocks is also slight in transverse direction. Similar to the case of longitudinal excitation, the damage of this studied bridge due to transversal main- and after-shocks can be also approximately obtained by superposing the independent results of main- and after-shocks.

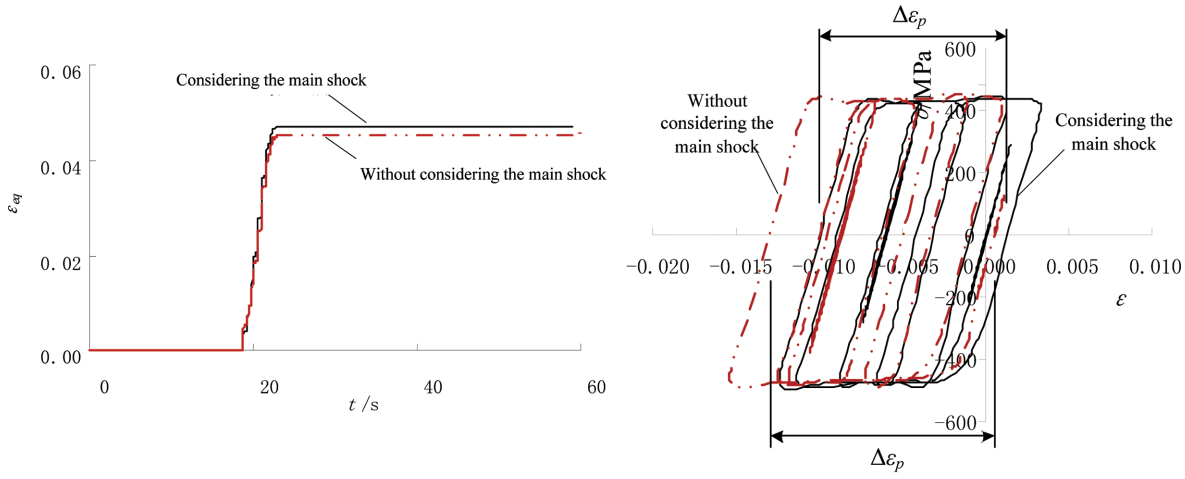

Fig. 15 The effect of transversal main shock damage on the strain responses of aftershock: (a) equivalent plastic strain and (b) stress-strain hysteretic curves

5. Conclusions

In this paper, the seismic responses of a steel-tower suspension bridge with a main span of 2000 m have been calculated under the main- and after-shock history records, using dynamic elasto-plastic finite displacement theory. Following conclusions are drawn:

(1) The damage caused by cumulative plastic strain can be ignored due to long natural period of the suspension bridge;
(2) Under the excitation of longitudinal earthquake, the tower shaft is prone to be injured at higher positions and at the shaft base;
(3) The transversal seismic response of the tower is similar to that of frame structures and it is vulnerable to seismic damage at the junctions between tower shafts and cross beams;
(4) When the intensity of an aftershock is not strong enough to cause plastic strain in the structure, the effect of the aftershock can be ignored in bridge seismic design;
(5) In the studied case, the effect of main shock induced damage on seismic response under aftershocks is so small that it can be ignored; therefore, the structural seismic damage of main- and after-shocks on bridges can be determined by superposing the damage indices under independent excitations of main- and after-shocks.

Acknowledgments

This study was supported by the Natural Science Foundation of China through the Grants No. 50908202/E080502 and No. 90915008/E080805. The digital data of ground motion accelerations of Chi-Chi Earthquake employed in this study are provided by the Center for Research on Earthquake Engineering of Taiwan, and those of Tokachi-oki Earthquake and Chuetus Earthquake are offered by Japan Meteorological Agency. These supports are gracefully acknowledged.

References

Abaqus. (2006), *ABAQUS, Version 6.5*, Habbitt, Karlsson & Sorensen, Inc., Pawtucket, R.I.

Amadio, C., Fragiacomo, M. and Rajgelj, S. (2003), "The effects of repeated earthquake ground motions on the non-linear response of SDOF systems", *Earthq. Eng. Struct. D.*, **32**(2), 291-308.

Fragiacomo, M., Amadio, C. and Macorini, L. (2004), "Seismic response of steel frames under repeated earthquake ground motions", *Eng. Struct.*, **26**(13), 2021-2035.

Franchin, P. and Pinto, P.E. (2009), "Allowing traffic over main shock-damaged bridges", *J. Earthq. Eng.*, **13**(5), 585-599.

George, P.C. "CHINA - Tangshan Earthquake of July 28, 1976", http://www.drgeorgepc.com/ Earthquake1976 ChinaTangshan.html.

Japan Meteorological Agency: http://www.jma.go.jp/index.html.

Japan Road Association. (2002), *Specifications for highway bridges*, Maruzen Co. Ltd., Tokyo.(in Japanese)

Kim, K.W., Chen, K.C., Wang, J.H. and Chiu, J.M. (2010), "Seismogenic structures of the 1999 Mw 7.6Chi-Chi,Taiwan,earthquake and its aftershocks", *Tectonophysics*, **489**(1-4), 119-127.

Kimura, Y., Kawano, K. and Nakamura, Y. (2007), "Effects on accumulated damages for seismic performance evaluation", *J. Earthq. Eng.-JSCE*, **53**(A), 398-405.

Lee, K. and Foutch, D.A. (2004), "Performance evaluation of damaged steel frame buildings subjected to seismic loads", *J. Earthq. Eng.*, **130**(4), 588-599.

Li, Q.W. and Ellingwood, B.R. (2007), "Performance evaluation and damage assessment of steel frame buildings under main shock-aftershock earthquake sequences", *Earthq. Eng. Struct. D.*, **36**(3), 405-427.

Luco, N., Bazzurro, P. and Cornell, C.A. (2004), "Dynamic versus static computation of the residual capacity of a main shock-damaged building to withstand an aftershock", *Proceedings of the 13th World Conference on Earthquake Engineering,* Vancouver, Canada.

McCabe, S.L. and Hall, W.J. (1989), "Assessment of seismic structural damage", *J. Earthq. Eng.*, **115**(9), 2166-2183.

Murata, A., Kitaura, M. and Miyajima, M. (2004), "Prediction of damage to structures through fatigue response spectra considering number of earthquake response cycles", *Proceedings of the 13th world conference on earthquake engineering*, Vancouver, Canada.

Park, Y.J. and Alfredo, H.S. (1985), "Mechanistic seismic damage model for reinforced concrete", *J. Earthq. Eng.*, **111**(4), 722-739.

Usami, T. (2007), *Guidelines for seismic and damage control design of steel bridges*, GIHODO SHUPPAN Co. Ltd., (in Japanese).

Zhao, B. and Taucer, F. (2010), "Performance of Infrastructure during the May 12, 2008 Wenchuan Earthquake in China", *J. Earthq. Eng.*, **14**(4), 578-600.

JL